J. Fluid Mech. (1999), *vol.* 394, *pp.* 193–203. Printed in the United Kingdom

© 1999 Cambridge University Press

Visualization of a mechanism for three-dimensional interaction and near-wall eruption

By C. V. SEAL AND C. R. SMITH

Department of Mechanical Engineering and Mechanics, Lehigh University, Bethlehem, PA 18015, USA

(Received 27 May 1998 and in revised form 22 March 1999)

An experimental configuration has been found which allows detailed observation of three-dimensional vortex–vortex and associated vortex–surface interactions which appear similar to those observed in fully turbulent flow. Hydrogen bubble visualization illustrates a complicated intertwining, or braiding, of two initially co-rotating vortices. It is observed that the three-dimensional interactions of the braided vortices induces a pair of local surface-fluid eruptions reminiscent of the 'bursting' behaviour characteristic of the near-wall regeneration process of fully turbulent boundary layers.

1. Introduction

One of the key features of a turbulent boundary layer is the regeneration process which allows turbulence to be self-sustaining/replicating in a naturally dissipative environment. A substantial amount of effort by numerous researchers (Panton 1997) has led to several proposed mechanisms to explain the observed self-replicating behaviour. One such mechanism consists of the so-called 'bursting', where the wall layer breaks down locally and erupts into the outer region. These eruptions intermittently feed plumes of concentrated vorticity into the outer region which subsequently roll up into new turbulent vortices (Smith & Walker 1997). Hence any complete structural model of turbulence must include all mechanisms by which this so-called 'bursting' occurs. The present paper presents hydrogen bubble visualizations of a unique flow situation which illustrates a mechanism which could help precipitate turbulent bursting in turbulent boundary layers as a result of the three-dimensional interaction of two discrete vortices and their associated interaction with the adjacent surface.

During the course of an investigation into the control of laminar junction flows (Seal 1997), it was observed that under appropriate conditions the application of spatially limited suction through a surface slot, located upstream of a cylinder–flat plate junction, modified the normally unsteady, laminar necklace vortex system (Seal *et al.* 1995; Greco 1990; Baker 1979) to a periodic system of intertwining vortices (figure 1*a*). For the Reynolds number used in this experiment, the baseline (no applied suction) laminar junction flow is characterized by the periodic formation of U-shaped necklace (or horseshoe) vortices upstream of the cylinder, which subsequently break away from the formation region and move downstream towards the cylinder. When the appropriate slot suction is applied, the system becomes characterized by the formation of a 'braid' structure shown schematically in figure 1(*a*). In this case, downstream of the suction slot necklace vortices periodically form and break away from the formation region in much the same manner as in the baseline case; however,

https://doi.org/10.1017/S0022112099005571 Published online by Cambridge University Press

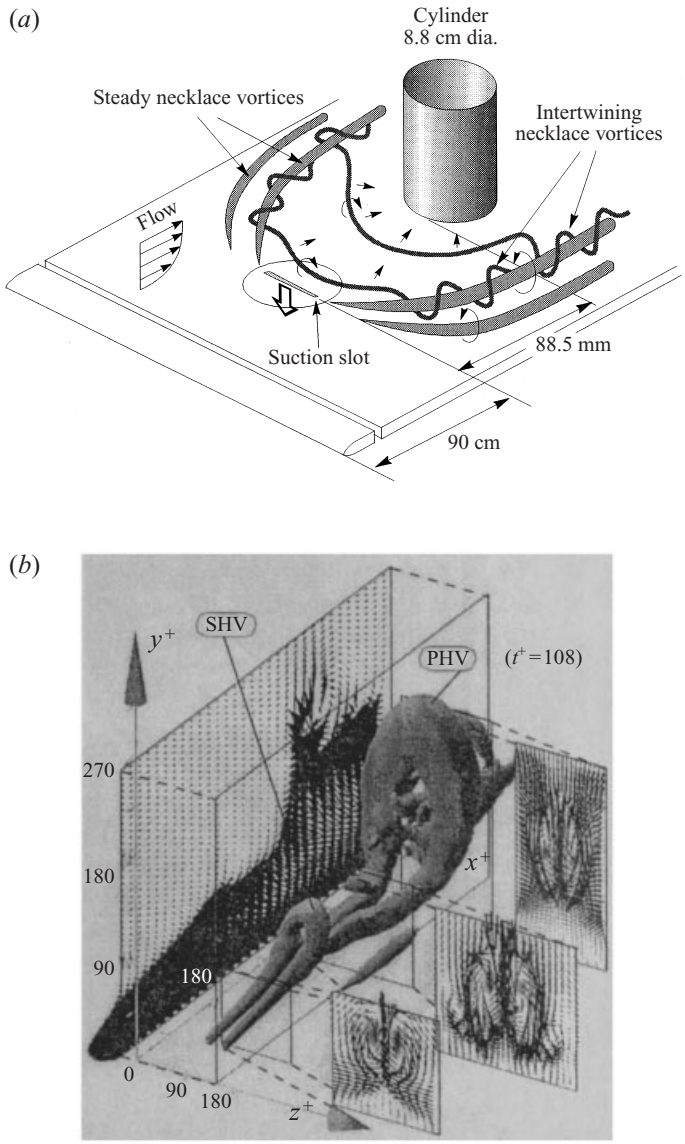


FIGURE 1. (*a*) Schematic illustrating the generation of the intertwining vortex system; slot located in the formation region. (*b*) Visualization of a hairpin packet illustrating the intertwining of two co-rotating vortices (from Zhou *et al.* 1997).

outboard of the symmetry plane the legs of these unsteady vortices intertwine with the leg of a steady vortex emanating from the outboard edges of the suction slot. Associated with this intertwining is a pair of local surface-fluid eruptions induced by the combined vortex–vortex interactions with the flat plate (described below), which appear similar to the bursts observed in turbulent boundary layers.

In addition to bursting, another important characteristic of turbulence, which is reproduced by the present system, is the three-dimensional interaction of turbulent vortical structures. In a fully turbulent boundary layer, the types of vortex–vortex interactions that may take place are myriad. However, recent analysis of Spalart's DNS

https://doi.org/10.1017/S0022112099005571 Published online by Cambridge University Press

data (Cantwell, Chacin & Bradshaw 1997) illustrates that the turbulent boundary layer contains a multitude of complex vortical structures, a number of which '... are tilted stream wise tubes inclined away from the wall that seem to bundle and twist, creating long braids'. Another instance where this vortex–vortex interaction can take the form of braiding is in the interaction of the legs of two adjacent hairpin vortices, which are generally regarded by many as a dominant structure of a turbulent boundary layer (e.g. Theodorson 1952; Smith *et al.* 1991; Robinson 1991; and Zhou *et al.* 1997). For example, figure 1(*b*) taken from the recent investigation of Zhou *et al.* (1997), seems to reflect this braiding, where the legs of a large primary hairpin vortex (PHV) intertwine with the legs of a secondary hairpin vortex (SHV).

The experimental system described in the present paper provides an ideal opportunity to perform a detailed study of two flow elements, or 'kernels' (Smith 1993), believed to play a major role in the dynamics of turbulent boundary layers, namely the aforementioned three-dimensional interaction of vortical structures and the subsequent generation of near-wall eruptions or bursts. It is the goal of such kernel studies to examine in detail the dynamic behaviour of important turbulent flow structures and repetitive patterns, which can be the source of relevant turbulent dynamics and kinematics, establishing their potential relevance to the overall turbulence process. The improved understanding of the process of mass/momentum exchange in turbulence production which these studies may provide could lead to more rational methods for control of turbulence and aid in the development of truly dynamic models.

2. Experimental apparatus and method

Experiments were performed in a Plexiglas free-surface water channel with a working test section 0.3 m deep by 0.9 m wide by 5.0 m long located in the Lehigh University Fluid Dynamics Research Laboratory (see Acalar & Smith 1987 for details). A 1.8 m long (1.9 cm thick) Plexiglas flat plate with a 5 : 1 elliptical leading edge was used to establish a laminar boundary layer (figure 1*a*). A circular cut-out was machined in the centre of the plate to accept an interchangeable suction slot insert at a streamwise location 90 cm from the leading edge; the plug used in the present study employed a 6.4 cm $\times$ 2 mm rectangular slot in a cross-stream orientation (see Seal & Smith 1999 for a detailed description of the suction slot). For the present experiment the suction rate was set to 1.89 ml s^{-1}, which translates to an average suction velocity of $V_{\text{suction}} = 1.49\,\text{cm}\,\text{s}^{-1}$. The free-stream velocity (U_∞) was set at 8.26 cm s^{-1}, giving a non-dimensional suction velocity of $V_{\text{suction}}/U_\infty = 0.18$.

A junction geometry was created by placing an 8.8 cm diameter cylinder directly on the flat plate (figure 1*a*). The length of the cylinder was such that it extends beyond the edge of the boundary layer, well into the free stream. To maintain symmetry, the cylinder was located on the centreline of the plate, in line with the suction slot insert. The cylinder was placed 8.85 cm downstream of the suction slot (figure 1*a*), which gives Reynolds numbers $Re_L = 7.8 \times 10^4$, and $Re_{\delta^*} = 481$, where Re_L and Re_{δ^*} are calculated for an equivalent, unobstructed, laminar boundary layer at the cylinder leading edge ($L = 98.85$ cm).

Flow visualization was performed using a moveable hydrogen bubble visualization probe consisting of a 25 µm diameter platinum wire soldered taut between two insulated brass rods forming a Y-shaped support. The probe was used in a cross-stream orientation to generate bubble sheets parallel to the flat plate surface; the wire location was varied according to how the flow was to be marked. Lighting consisted

https://doi.org/10.1017/S0022112099005571 Published online by Cambridge University Press

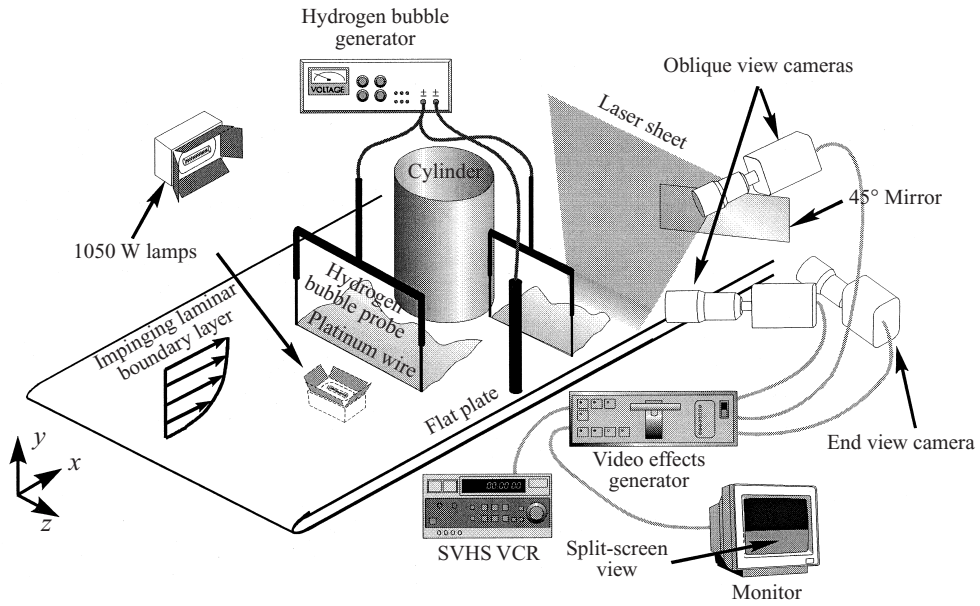


FIGURE 2. Schematic of the flow visualization apparatus.

of general illumination through the bottom or from the side of the channel using a 1050 W photographic lamp. See figure 2.

The flow visualization experiments were recorded in real time using a colour video camera and an SVHS video cassette recorder. The recorder is capable of playing the video either forwards or backwards, in slow motion or freezing a selected frame. A single-frame advance mode was also used to allow detailed analysis of the experiments. Single images from a video sequence could be digitized into a TIFF file format via a video frame-grabber board.

For selected instances, simultaneous, two-camera, dual-view hydrogen bubble visualizations were performed. Here two cameras were used simultaneously, one with an oblique view and the other with either an end view (through the use of a 45° mirror located downstream of the cylinder) or a low-angle side view (see figure 2). A video effects generator was used to combine the two video signals in a split-screen view. For these visualizations, general illumination was used for the oblique views and a cross-stream laser sheet was used to illuminate the bubble sheet for end views.

3. Results and discussion

The flow topology of this system is characterized by the previously described braid system, shown schematically in figure 1(*a*), characterized by an advecting vortex intertwined (or braided) around a relatively steady necklace vortex. Downstream of the slot, on the symmetry plane, an unsteady necklace vortex system in the breakaway regime (see Seal *et al.* 1995) develops. Around the sides of the cylinder these unsteady vortices fully intertwine with a steady vortex (which is part of a steady two-vortex system) which originates from the outboard edges of the suction slot; this braiding is clearly shown in figure 3 by the hydrogen-bubble-marked vortex cores.

Note that because these vortices are regions of low pressure, hydrostatic forces cause the hydrogen bubbles to concentrate in the vortex cores. During the study, the

https://doi.org/10.1017/S0022112099005571 Published online by Cambridge University Press

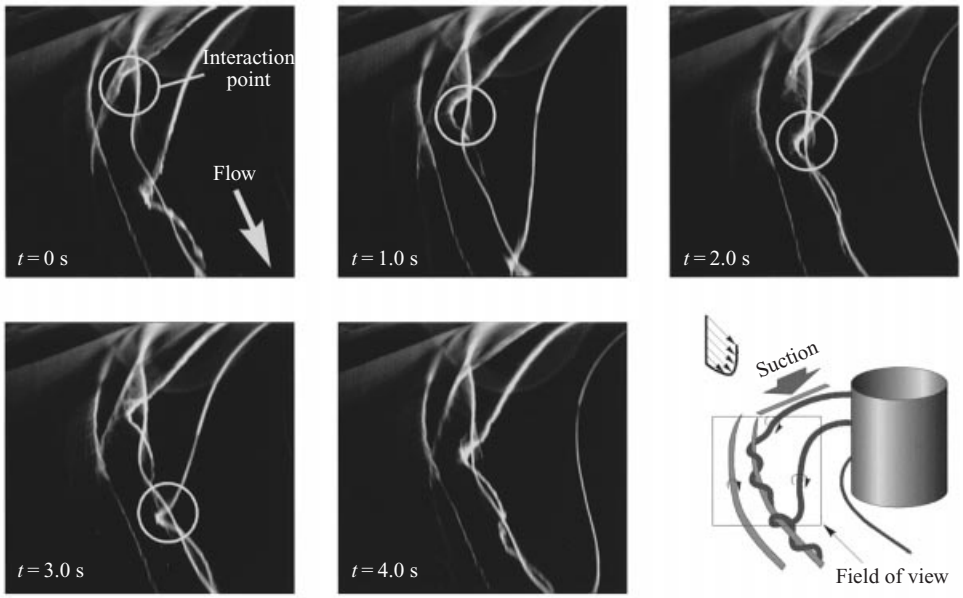


FIGURE 3. Magnified hydrogen bubble time sequence illustrating the periodic three-dimensional intertwining of the necklace vortices resulting from moderate suction applied in the formation region of an unsteady, laminar necklace vortex system. Hydrogen bubble wire located 50 mm upstream of the cylinder and 4 mm off the surface. $U_\infty = 8.26\,\mathrm{cm\,s^{-1}}$, $Re_L = 7.8 \times 10^4$, and $Re_{\delta^*} = 481$, where Re_L and Re_{δ^*} are calculated for an equivalent, unobstructed, laminar boundary layer at the cylinder location L.

position of the hydrogen bubble wire was systematically varied and the characteristics of the local flow closely examined to ensure that the visualized structures were fully rotational vortices. The position of the bubble wire was then optimized to ensure that the generated bubbles were entrained into, and visualized the core of, the interacting vortices.

Figures 3 and 4 show time sequences illustrating the temporal details and periodicity of the flow during this braiding process. Figure 3 is a magnified view of the initial intertwining of the vortices, and figure 4 is a more general view illustrating the downstream flow behaviour. As time progresses, the unsteady vortex develops in the usual laminar breakaway manner, moving towards the cylinder and into the corner region. During this process, the point where the unsteady and steady vortices meet (termed the 'interaction point', see figure 3) moves downstream and undergoes a rather complicated development and interaction with the surface (see below). The events described above are periodic, occurring in conjunction with the periodic vortex formation process.

Note that end-view visualizations of the intertwining vortices (not presented here) indicate that within the vortex braid each of the vortices maintains rotational motion, with vortex diameters of roughly 4 mm and strengths of $\Gamma/\nu \approx 400$. While the braiding process develops in a complicated three-dimensional manner, when the intertwining vortices comprising the braids are oriented in their predominant parallel (streamwise) configuration, the intertwining vortices will display spacings on the order of 5–8 mm, with typical rates of co-rotation of $\frac{1}{2}$ to 1 revolution per second.

Since both interacting vortices have the same sense of rotation, the predominant portion of the braiding is dominated by a process of mutual interaction and co-

https://doi.org/10.1017/S0022112099005571 Published online by Cambridge University Press

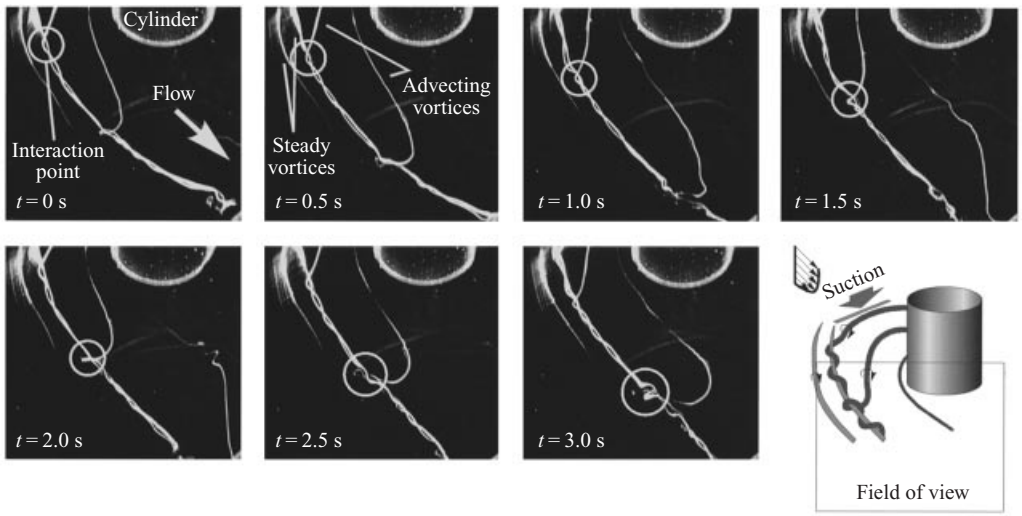


FIGURE 4. Oblique hydrogen bubble time sequence illustrating the temporal details of the downstream flow behaviour of the intertwining necklace vortices. Hydrogen bubble wire located 50 mm upstream of the cylinder and 4 mm off the surface. Same conditions as figure 3.

rotation. However, at periodically occurring interaction points, indicated by the circles in figures 3 and 4, the two vortices initiate a complicated three-dimensional interaction (illustrated in figure 4) in which the key feature appears to be the turning of the advecting vortex. Initially, both the steady and advecting vortices share the same sense of rotation and essential streamwise orientation relative to the mean flow (see the upper left picture of figure 4, $t = 0$). However, as the interaction points move downstream, the portion of the advecting vortex nearest the interaction point reorients its axis of rotation through an angle of approximately 90°. A possible explanation for this behaviour is the initial orientation of the advecting vortex, which is initially closest to the plate (beneath the steady vortex) at the interaction point, and at $\sim 45°$ to the steady vortex (see figure 4, $t = 1.0$ s), giving it a cross-stream orientation. In view of the rotational sense of the advecting vortex, the convection velocity of the interaction point would, therefore, be reduced relative to the mean convection velocity due to the influence of the image of the advecting vortex. Another possible explanation is that the suction slot, by removing a portion of the low-momentum boundary layer fluid and causing higher-momentum outer fluid to divert towards the flat plate surface upstream of the cylinder, could cause an acceleration of the inboard fluid (i.e. the fluid closer to the cylinder) relative to the outboard flow, thus promoting the reorientation of the advecting vortex. However, whatever the cause of the reorientation of the axis of rotation of the advecting vortex, once the turning takes place, the two interacting vortices have opposing senses of rotation that result in the induced motion of the vortices toward the surface, which ultimately results in their subsequent interaction with the surface, as described below.

Note that the braiding behaviour described here was studied in detail for the indicated Reynolds numbers of $Re_L = 7.8 \times 10^4$, and $Re_{\delta^*} = 481$, with the suction slot location located in what is termed the formation region for naturally occurring necklace vortex systems. Because the overall study (Seal 1997) examined a matrix of suction slot strengths and locations relative to the vortex formation region, the braiding behaviour was examined in detail for only the one set of Reynolds numbers.

https://doi.org/10.1017/S0022112099005571 Published online by Cambridge University Press

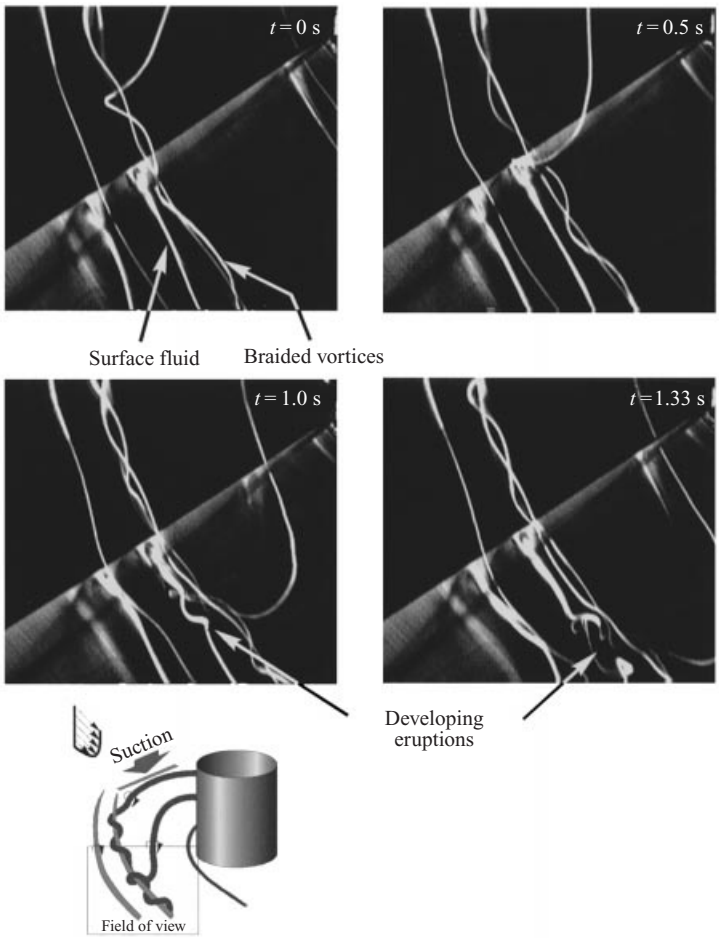


FIGURE 5. Magnified, oblique-view hydrogen bubble time sequence illustrating the periodic three-dimensional intertwining of the necklace vortices and the resultant surface interactions. Visualization was performed with two bubble wires: one upstream, marking the vortex cores (50 mm upstream of the cylinder and 4 mm off the surface), and a second located on the surface at the cylinder centreline, marking the surface fluid. Same conditions as figure 3.

However, it was apparent from other exploratory studies that similar braiding-type behaviour is present for other combinations of Reynolds numbers and suction rates, although systematic studies were not conducted.

As the process of mutual induction moves the reoriented vortices into closer proximity to the surface, an interaction of the vortices with the surface fluid develops, culminating in the generation of focused, localized eruptions of surface fluid. This strong vortex–surface fluid interaction process is similar to the process predicted by the simulation studies of Peridier, Smith & Walker (1991), although the present behaviour is markedly more complicated and three-dimensional.

Figure 5 is a visualization of this process of vortex–surface fluid interaction using two separate hydrogen bubble wires (as shown in figure 2). One wire was located upstream of the cylinder (out of the field of view in figure 5), marking the vortex cores. A second wire was located on the flat plate surface (one radius downstream from the cylinder leading edge) to mark the surface fluid behaviour. In figure 5 this

https://doi.org/10.1017/S0022112099005571 Published online by Cambridge University Press

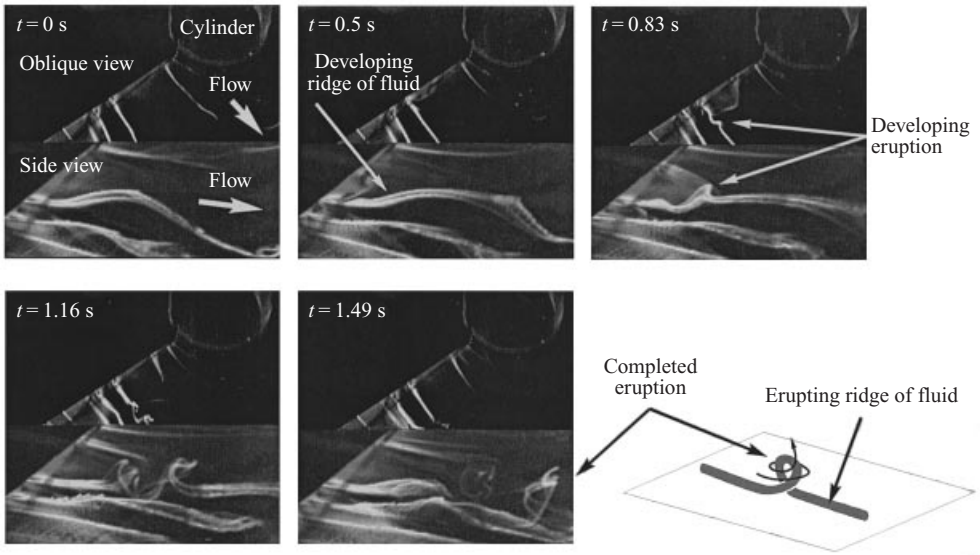


FIGURE 6. Simultaneous oblique- and side-view hydrogen bubble time sequence illustrating the surface eruptions induced by the intertwining vortices. Hydrogen bubble wire located on the surface at the cylinder centreline. Same conditions as figure 3.

second wire slants diagonally from the upper right edge to the lower left edge of the pictures. As the visualizations in figure 5 reveal, from $t = 0$ to 0.5 s the surface flow is characterized by a ridge of erupting fluid created by the interaction of the downstream extensions of the intertwining vortices with the surface (see Smith *et al.* 1991 for a more detailed description of this type of phenomenon). As the interaction point advects and develops downstream ($t = 1.0$ and 1.33 s), a pair of localized eruptions of surface fluid develops. Figure 5 seems to illustrate that the eruptive behaviour is linked in some way to the vortex turning described above, since the eruptions develop after the advecting vortex has undergone its rotation and movement toward the surface.

Figure 6 is a closer, simultaneous dual-view visualization of the eruption process described above, obtained using only the downstream surface wire. The top portions of the pictures are oblique views of the surface flow and the bottom portions are more magnified shallow-angle oblique views (essentially side views) of the same flow. An erupting ridge of fluid generated by the interaction of the intertwined vortices with the plate surface is clearly seen at $t = 0$ and 0.5 s. The subsequent development of the eruption is illustrated from $t = 0.83$ to 1.49 s, with the eruption essentially complete by $t = 1.49$ s.

The lower side views in figure 6 illustrate the rapid development of these eruptions from the initial ridge of fluid and also reveal their rotational nature, as illustrated by the upward spiralling of the hydrogen bubbles, which when viewed from above indicated a counterclockwise rotation. This rotation is likely to be a result of a re-orientation of the resident streamwise vorticity in the eruptive surface fluid. It is significant that from an end view (downstream of the initial eruption), the hydrogen bubbles marking the eruptions displayed a mushroom-shaped pattern similar to the patterns observed for isolated hairpin vortices (e.g. Acalar & Smith 1987) and in visualization studies of fully turbulent boundary layers (Head & Bandyopadhyay 1981).

https://doi.org/10.1017/S0022112099005571 Published online by Cambridge University Press

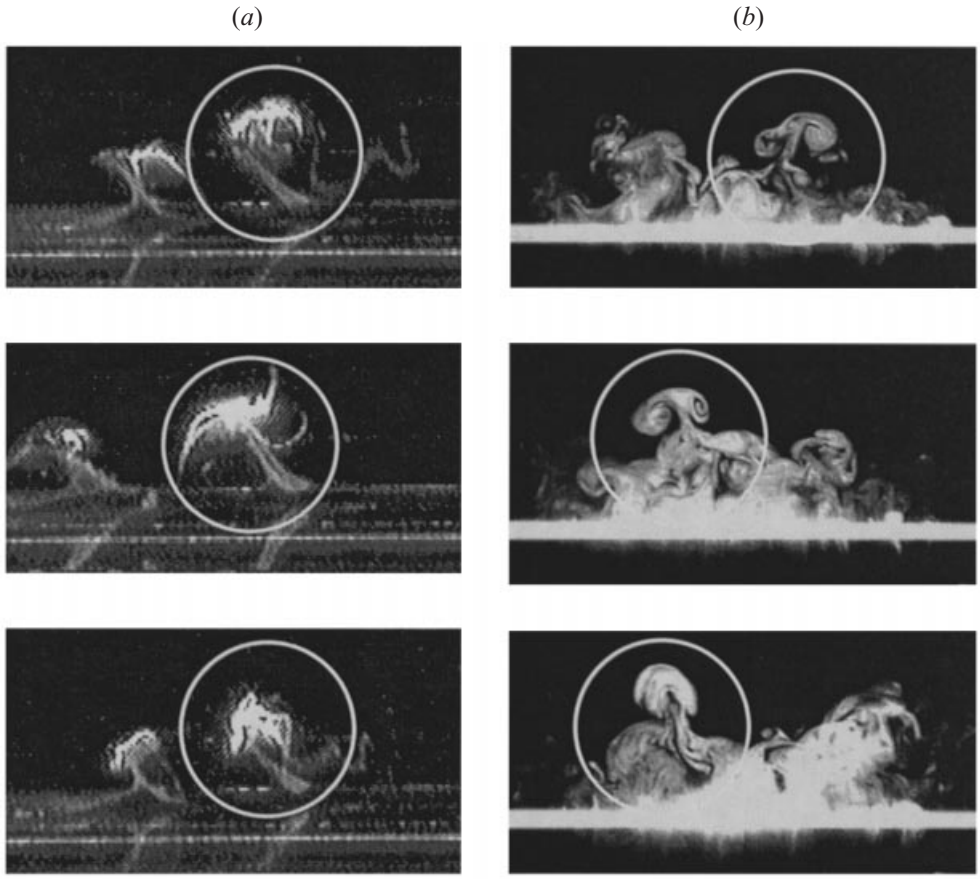


FIGURE 7. (*a*) End-view hydrogen bubble visualization of the mushroom-shaped patterns generated by the intertwining vortex–surface interaction (bubbles marking the surface fluid; laser sheet 10.9 cm downstream of the leading edge of the cylinder). (*b*) Selected laser-sheet smoke visualizations of a low-Reynolds-number turbulent boundary layer, $Re_\theta = 892$ (Wallace & Balint 1990).

Figure 7(*a*) shows several end views of the observed eruptions, obtained via a cross-stream laser sheet, which reveal the mushroom-shaped patterns described above (the larger structures indicated by circles on the pictures). Note that the smaller eruptive structures on the left side of the pictures are apparently caused by the surface interaction of a steady secondary vortex emanating from the edge of the suction slot (see figure 1*a*). Figure 7(*b*) is selected end-view laser-sheet smoke visualizations of a turbulent boundary layer (Wallace & Balint 1990), which exemplify the typical mushroom-type patterns observed in near-wall turbulence, and bear remarkable similarity to the patterns shown in figure 7(*a*).

Of further interest is the fact that these eruptive events often occur in sequential pairs (see figures 5 and 6), suggesting that one discrete vortex–vortex interaction (in proximity to a surface) can lead to the generation of two or more new flow structures. Along these lines, a recent investigation by Zhou *et al.* (1997) indicates that the more prevalent mode of existence of hairpin vortices in a turbulent boundary layer is in packets containing several hairpins of different scales. It could be that the double eruption mechanism observed in this study plays some role in the observations of

https://doi.org/10.1017/S0022112099005571 Published online by Cambridge University Press

Zhou *et al.*, which suggests that an initial hairpin vortex may naturally spawn a packet of vortices (i.e. several vortices existing simultaneously within a spatial envelope).

4. Conclusions

A unique experimental configuration has been discovered which allows detailed observation of three-dimensional vortex–vortex and associated vortex–surface interactions that appear similar to those observed in a turbulent boundary layer. The observed vortex behaviour illustrates a complicated intertwining, or braiding of two initially co-rotating vortices. It is observed that the three-dimensional interactions of the braided vortices induce a pair of local surface-fluid eruptions reminiscent of the near-wall bursting that is characteristic of the near-wall regeneration process for fully turbulent boundary layers.

The visualizations shown in the present paper demonstrate how turbulent-like eruptive behaviour can result from the three-dimensional interaction and deformation of intertwining vortices, suggesting a possible mechanism for similar behaviour in fully turbulent flow. That comparable mechanisms of vortex deformation and interaction may play a role in the process of turbulence regeneration is supported by several recent investigations into the nature of turbulence (e.g. Zhou *et al.* 1997 and Cantwell *et al.* 1997) which illustrate comparable situations where the intertwining of two vortices appears to occur in the turbulence process.

Clearly the phenomena described in the present paper are very complex and need to be investigated further to more fully understand how the observed events (i.e. intertwining vortices leading to surface eruptions) relate to naturally turbulent flow. The type of experimental configuration described here is an opportune system for such 'kernel' studies (Smith 1993) since the generated vortices are embedded in a three-dimensional laminar boundary layer, such that vortex–vortex and vortex–surface interactions can be observed free of the background turbulent fluctuations which make the detection and observation of such behaviour in a fully turbulent flow very difficult. Additionally, the remarkable periodicity and spatial repeatability of the intertwining and eruptive events generated by the present geometry and flow would greatly facilitate the use of sophisticated quantitative experimental techniques, such as holographic PIV, for the study of these complicated three-dimensional processes.

The authors wish to thank the Air Force Office of Scientific Research (AFOSR) for their support of this research under contracts: F49620-93-1-0346 and F49620-93-1-0217.

REFERENCES

Acarlar, M. S. & Smith, C. R. 1987 A study of hairpin vortices in a laminar boundary layer. Part 1. Hairpin vortices generated by hemisphere protuberances. *J. Fluid Mech.* **175**, 1–41.

Baker, C. J. 1979 The laminar horseshoe vortex. *J. Fluid Mech.* **95**, 347–367.

Cantwell, B. J., Chacin, J. M. & Bradshaw, P. 1997 On the dynamics of turbulent boundary layers. In *Self-Sustaining Mechanisms of Wall Turbulence* (ed. R. L. Panton), pp. 365–384, Computational Mechanics Publications, Southampton, UK.

Greco, J. J. 1990 The flow structure in the vicinity of a cylinder-flat plate junction: flow regimes, periodicity, and vortex interactions. MS thesis, The Department of Mechanical Engineering, Lehigh University, Bethlehem, PA.

Head, M. R. & Bandyopadhyay, P. 1981 New aspects of turbulent boundary layer structure. *J. Fluid Mech.* **107**, 297–338.

https://doi.org/10.1017/S0022112099005571 Published online by Cambridge University Press

Panton, R. L. (Ed.) 1997 *Self-Sustaining Mechanisms of Wall Turbulence*. Computational Mechanics Publications, Southampton, UK.

Peridier, V. J., Smith, F. T. & Walker, J. D. A. 1991 Vortex-induced boundary-layer separation. Part 1. The unsteady limit problem $Re \rightarrow \infty$. *J. Fluid Mech.* **232**, 99–131.

Robinson, S. K. 1991 Coherent motions in a turbulent boundary layer. *Ann. Rev. Fluid Mech.* **23**, 601–639.

Smith, C. R., Walker, J. D. A., Haidari, A. H. & Sabrun, Ü. 1991 On the dynamics of near-wall turbulence. *Phil. Trans. R. Soc. Lond.* A **336**, 131–175

Seal, C. V. 1997 The control of junction flows. PhD dissertation, The Department of Mechanical Engineering, Lehigh University, Bethlehem, PA.

Seal, C. V. & Smith C. R. 1999 The control of turbulent end-wall boundary layers using surface suction. *Exps. in Fluids* (in press).

Seal, C. V., Smith, C. R., Akin, O. & Rockwell, D. 1995 Quantitative characteristics of a laminar, unsteady necklace vortex system at a rectangular block-flat plate juncture. *J. Fluid Mech.* **286**, 117–135.

Smith, C. R. 1993 Use of 'kernel' experiments for modeling of near-wall turbulence. In *Near-Wall Turbulent Flows* (ed. R. M. C. So, C. G. Speziale, & B. E. Launder), pp. 33–42. Elsevier.

Smith, C. R. & Walker, J. D. A. 1997 Sustaining mechanisms of turbulent boundary layers: the role of vortex development and interactions. In *Self-Sustaining Mechanisms of Wall Turbulence* (ed. R. L. Panton), pp. 13–47. Computational Mechanics Publications, Southampton, UK.

Theodorsen, T. 1952 Mechanism of turbulence. In *Proc. Second Midwestern Conference on Fluid Mechanics*. Bull. 149, Ohio State University, Columbus, OH.

Wallace, J. M. & Balint, J. L. 1990 Flow visualization study of the effects of trip type on the structure of the turbulent boundary layer. Video Tape, Turbulence Laboratory, University of Maryland.

Zhou, J., Adrian, R. J., Balachandar, S. & Kendall, T. M. 1997 Mechanisms for generating coherent packets of hairpin vortices in near-wall turbulence. *TAM Rep.* 856 The Department of Theoretical and Applied Mechanics, The University of Illinois at Urbana-Champaign, Urbana-Champaign, IL.

https://doi.org/10.1017/S0022112099005571 Published online by Cambridge University Press